# Quasi-local evolution of cosmic gravitational clustering in weakly non-linear regime

Jesús Pando,<sup>1</sup> Longlong Feng<sup>2</sup> and Li-Zhi Fang<sup>3</sup>

## ABSTRACT

We investigate the weakly non-linear evolution of cosmic gravitational clustering in phase space by looking at the Zel'dovich solution in the discrete wavelet transform (DWT) representation. We show that if the initial perturbations are Gaussian, the relation between the evolved DWT mode and the initial perturbations in the weakly non-linear regime is quasi-local. That is, the evolved density perturbations are mainly determined by the initial perturbations localized in the same spatial range. Furthermore, we show that the evolved mode is monotonically related to the initial perturbed mode. Thus large (small) perturbed modes statistically correspond to the large (small) initial perturbed modes. We test this prediction by using QSO Ly $\alpha$  absorption samples. The results show that the weakly non-linear features for both the transmitted flux and identified forest lines are quasi-localized. The locality and monotonic properties provide a solid basis for a DWT scale-by-scale Gaussianization reconstruction algorithm proposed by Feng & Fang (Feng & Fang, 2000) for data in the weakly non-linear regime. With the Zel'dovich solution, we find also that the major non-Gaussianity caused by the weakly non-linear evolution is local scale-scale correlations. Therefore, to have a precise recovery of the initial Gaussian mass field, it is essential to remove the scale-scale correlations.

Subject headings: cosmology: theory - large-scale structure of the universe

## 1. Introduction

One of the basic goals of large scale structure study is to reconstruct the initial mass field of the universe. Assuming observed objects trace the underlying matter field in some

<sup>&</sup>lt;sup>1</sup>Department of Chemistry and Physics, Chicago State University, Chicago, IL 60628

<sup>&</sup>lt;sup>2</sup>Center for Astrophysics, University of Science and Technology of China, Hefei, Anhui 230026, National Astronomical Observatories, Chinese Academy of Science, Chao-Yang District, Beijing, 100012, P.R. China

<sup>&</sup>lt;sup>3</sup>Department of Physics, University of Arizona, Tucson, AZ 85721

way, it should be possible to recover the initial conditions of the mass field. For instance, if the probability distribution function (PDF) of the initial mass fluctuations is Gaussian, one may recover the initial Gaussian mass fluctuations by properly removing all non-Gaussian features via the Gaussianization reconstruction algorithm (Weinberg 1992.)

The key step in the Gaussianization algorithm is a mapping from a smoothed observed non-Gaussian distribution of the density contrast,  $\delta(x) = (\rho - \bar{\rho})/\bar{\rho}$  ( $\rho$  is the mass density, and  $\bar{\rho}$  is its mean) into a smoothed initial Gaussian density contrast  $\delta_0(x)$ . The basic assumptions of this mapping are that the relation between  $\delta(x)$  and the initial density distribution  $\delta_0(x)$ is local and monotonic, i.e., the rank order of the mass density field, smoothed over a given scale, is preserved even under nonlinear gravitation evolution(Narayanan & Weinberg 1998). Thus, the high initial density pixels will evolve into high  $\delta(x)$  pixels and low initial density pixels into low  $\delta(x)$  pixels. With this assumption, the Gaussian mapping can be realized by a point-to-point, order-preserving transformation. The shape of the initial Gaussian density field is recovered with an arbitrary normalization.

This method has been employed to recover the initial mass field and power spectrum from galaxy redshift surveys and from the transmitted flux of the Ly $\alpha$  absorption in QSO spectra (Croft et al. 1998.) The validity of the point-to-point (or pixel-to-pixel) recovery of the initial Gaussian mass field from the evolved mass field stems from the belief that the transmitted flux probably is a pixel-to-pixel tracer of the underlying dark matter distribution (Bi 1993; Fang et al. 1993; Bi, Ge & Fang 1995; Hernquist et al 1996; Bi & Davidsen 1997; Hui, Gnedin & Zhang 1997.)

However, whether the order-preserving assumption is reasonable is far from clear. It has been argued that the order-preserving condition may be a poor approximation to the actual dynamics because of the non-locality of gravitational evolution (Monaco & Efstathiou 2000). Gravitational clustering is not localized. Even in the weakly non-linear evolutionary regime, the processes of cosmic clustering typically are those of objects free falling into potential wells (e.g. Xu, Fang & Wu 2000), Fourier mode-mode coupling (e. g. Suto & Sasaki 1991), and the merging of pre-virialized dark halos. These processes are generally *non-local*.

In the Zel'dovich approximation (Zel'dovich 1970), the density field  $\rho(\mathbf{x}, t)$  at (Eulerian) comoving position  $\mathbf{x}$  and time t is determined by the initial perturbation at (Lagrangian) comoving position,  $\mathbf{q}$ , plus a displacement  $\mathbf{S}$ :

$$\mathbf{x}(\mathbf{q},t) = \mathbf{q} + \mathbf{S}(\mathbf{q},t). \tag{1}$$

The displacement  $\mathbf{S}(\mathbf{q}, t)$  represents the effect of density perturbations on the trajectories of gravitating particles. Therefore, cosmic self-gravitating systems do not follow a Eulerian *point-to-point* localized evolution. Even when the transmitted flux is locally determined by the evolved underlying dark matter distribution, the relation between the initial mass field and the transmitted flux might still be non-local. The initial power spectrum reconstructed from the point-to-point Gaussian mapping of  $Ly\alpha$  transmitted flux shows a systematic suppression on small scales (Croft et al. 1999.) This problem may be mitigated by smoothing the data. However, the smoothing scale is put in by hand and it is hard to understand how this scale can be determined from the dynamics of the non-local evolution. For these reasons the basis of the order-preserving transformation and the point-to-point Gaussian mapping need to be reconsidered.

In this paper, we will show first that the assumption of point-to-point locality is not necessary for a proper Gaussianization reconstruction.

Recently, we showed that the transmitted flux Gaussianized by the point-to-point Gaussian mapping is still largely non-Gaussian (Feng & Fang 2000.) That is, the non-Gaussianities of the original transmitted flux are retained in the mass field recovered by the point-to-point, order-preserving transformation. Especially troubling is the fact that the scale-scale correlations of the Gaussianized field are about the same as before the mapping. The mass power spectrum recovered by the point-to-point Gaussian mapping is systematically lower than the initial mass spectrum on scales at which the scale-scale correlation of the recovered mass field are substantial.

To solve this problem, a scale-by-scale algorithm of the Gaussian mapping was proposed (Feng & Fang 2000.) In this algorithm the order-preserving transformation is done on the coefficients of a space-scale decomposition rather than on each pixel of the transmitted flux. This method can effectively remove the non-Gaussianities of the observed distribution, especially clearing the scale-scale correlations. Consequently, small scale suppression is significantly reduced. Furthermore, the scale-by-scale Gaussianization procedure does not require a point-to-point order preservation, but only the order preservation of the density fluctuations of the space-scale decomposed field.

We will show that the order preservation assumption for the scale-by-scale Gaussian mapping is supported by the Zel'dovich approximation and that in quasi-linear evolution, the gravitational clustering is quasi-local and monotonic. Moreover, we will find that the non-Gaussian features during the weakly non-linear regime are dominated by the local scalescale correlations. Therefore, at least for the transmitted flux and forest lines of the QSO  $Ly\alpha$  absorption spectrum, the scale-by-scale Gaussianization algorithm has a solid basis in the weakly non-linear regime.

The paper is organized as follows: Section 2 presents the quasi-locality condition needed for the scale-by-scale Gaussianization recovery. In Section 3 we show the quasi-locality and monotonic nature of the weak non-linear evolution using the Zel'dovich solution of the growth modes. Section 4 presents the result of measuring the quasi-locality for samples of the Ly $\alpha$ absorption spectrum. The conclusions are summarized in Section 5.

## 2. Scale-by-scale Gaussian mapping and the quasi-locality condition

### 2.1. Problems with the point-to-point Gaussian mapping

Let us briefly introduce the algorithm for a point-to-point Gaussian mapping which is designed for recovering the initial Gaussian mass density contrast  $\delta_0(\mathbf{x})$  from an observed, non-Gaussian distribution  $\delta(\mathbf{x})$ . As an example, we consider an observed transmitted flux F or absorption optical depth  $\tau = -\ln F$  of the Ly $\alpha$  absorption in QSO spectra. The distribution is one-dimensional and of length L. The PDF of the observed transmitted flux Fis generally non-Gaussian, while the PDF of the initial density contrast  $\delta_o$  is assumed to be Gaussian in a large variety of structure formation models. The relation between  $F = e^{-\tau}$ and  $\delta_0$  is assumed to be order-preserved, or monotonic, i.e., high initial density  $\delta_0$  pixels evolve into high absorption optical depth  $\tau$  pixels, while low initial density pixels into low  $\tau$  pixels. Thus, a point-to-point (or pixel-to-pixel) Gaussian mapping can be done as follows. First, sort in ascending order, the N pixels by the observed amount of flux. Second, assign to the n-th pixel a density contrast  $\delta$  by the solving the error function equation  $(2\pi)^{-1/2} \int_{-\infty}^{\delta} \exp(-x^2/2) dx = n/N$ . This pixel-to-pixel Gaussian mapping produces a mass field with the same rank order as the original flux but with a Gaussian PDF. After determining the overall amplitude of the Gaussian mapped field by a separate procedure, the initial density field  $\delta_0$  is recovered (Weinberg 1992.)

However, the density field recovered by the pixel-to-pixel Gaussian mapping still exhibits non-Gaussian features. Especially, the scale-scale correlations of the Gaussianized field are almost as strong as the pre-Gaussianized flux. The pixel-to-pixel Gaussian mapping does not remove all the non-Gaussianities and the initial Gaussian field will not be recovered precisely. The power spectrum recovered by the point-to-point Gaussian mapping is systematically lower than the initial mass spectrum on scales at which the scale-scale correlation is substantial. Physically, the effect might just be due to the fact that  $\delta$  is simply too non-linear, and the relation between  $\delta$  and  $\delta_0$  is no longer monotonic. If this is the case, then a scale-adaptive smoothing is required before Gaussianization.

However, a smoothing window function sometimes introduces spurious features. For instance, the aliasing of the power spectrum on scales around the Nyquist frequency corresponds to the scale of the smoothing grid. However with the DWT analysis one need not introduce window functions for smoothing because the scaling functions of the wavelet transform already play that role. The scaling function is orthogonal to the relevant wavelets. False correlations due to the smoothing window can then be perfectly eliminated (Feng & Fang 2000.) Therefore, a scale-adaptive smoothing and reconstruction can be realized by the scale-by-scale Gaussian mapping.

#### 2.2. Scale-by-scale Gaussian mapping

Scale-by-scale, or scale-adaptive Gaussianization can be performed via the discrete wavelet transform  $(DWT)^4$ . The first step in this process is to wavelet expand the flux F as

$$F(x) = \bar{F} + \sum_{j=0}^{\infty} \sum_{l=0}^{2^{j}-1} \tilde{\epsilon}_{j,l} \psi_{j,l}(x)$$
(2)

where  $\psi_{j,l}(x)$ ,  $j = 0, 1, ..., l = 0...2^j - 1$ , is an orthogonal and complete basis. The wavelet basis (mode)  $\psi_{j,l}(x)$  is localized both in physical space and in Fourier (scale) space. The function  $\psi_{j,l}(x)$  is centered at position  $lL/2^j$  in physical space and at wavenumber  $2\pi \times 2^j/L$ in Fourier space. The wavelet function coefficients (WFCs),  $\tilde{\epsilon}_{j,l}$ , are labeled by the two subscripts j and l corresponding to the scale and position respectively. The  $\tilde{\epsilon}_{j,l}$  describe the fluctuation of the flux on scale  $L/2^j$  at position  $lL/2^j$  and are computed as the inner product

$$\tilde{\epsilon}_{j,l} = \int_0^L F\psi_{j,l} dx.$$
(3)

The density fields in cosmology are assumed to be ergodic, that is, the average over an ensemble is equal to the spatial average taken over *one* realization. This is the so-called fair sample hypothesis (Peebles 1980). A homogeneous Gaussian field with a continuous power spectrum is certainly ergodic(Adler 1981). In some non-Gaussian cases, such as homogeneous and isotropic turbulence, ergodicity also approximately holds(Vanmarke, 1983). Roughly, the ergodic assumption is reasonable if the spatial correlations decrease sufficiently rapidly with increasing separation. This property can effectively be used by the DWT because the wavelet  $\psi_{j,l}(x)$  are orthogonal with respect to the position index l. The SFCs  $\tilde{\epsilon}_{j,l}$   $(j = 0...2^j - 1)$  can be considered as  $2^j$  independent sampling, without false correlations caused by a non-orthogonal or redundant decomposition. Thus, for ergodic random fields the  $2^j$  WFCs form

<sup>&</sup>lt;sup>4</sup>For the details of the DWT refer to the classic papers by Mallat (1989a,b); Meyer (1992); Daubechies, (1992) and references therein, and for physical applications, refer to Fang & Thews (1998) and references therein.

a statistical ensemble on scale j. So for quantity  $X_j$ , the ensemble average is given by

$$\langle X_j \rangle \simeq \frac{1}{2^j} \sum_{l=0}^{2^j - 1} X_{j,l} \tag{4}$$

where  $X_{j,l}$  is the quantity at position l. In other words, the distribution of the  $2^j$  WFCs is the one-point distribution of  $X_j$ .

In short we have arrived at the scale-by-scale Gaussianization algorithm which consists of the following steps: 1.) Sort out the  $2^j$  WFCs,  $\tilde{\epsilon}_{j,l}$ , of the flux field F in ascending order. 2.) Assign to the  $2^j$  WFCs, the Gaussianized density contrast  $\delta^g$  at position l by the solving the error function equation. In this algorithm, the order-preserving transformation is performed scale-by-scale. It gives a position(l)-to-position(l) Gaussian mapping for each scale j. After a proper amplitude normalization (Feng & Fang 2000), the initial Gaussian density field  $\delta_0$  is reconstructed with the Gaussianized WFCs  $\tilde{\epsilon}_{j,l}^g$  (we have added the subscript g to emphasize that we are dealing with a Gaussian field.)

The  $\tilde{\epsilon}^g_{i,l}$  are normally distributed with covariance given by

$$\langle \tilde{\epsilon}^g_{j,l} \tilde{\epsilon}^g_{j',l'} \rangle = P_{j,l} \delta_{j,j'} \delta_{l,l'}. \tag{5}$$

For a homogeneous Gaussian field,  $P_{j,l}$  is *l*-independent, i.e.,  $P_{j,l} = P_j$ . Thus,  $P_j$  is the power spectrum of the initial field. (Pando & Fang 1998b, Feng & Fang 2000, Fang & Feng, 2000.) Because the  $2^j$  WFCs  $\tilde{\epsilon}_{j,l}^g$  form a fair ensemble, the DWT power spectrum  $P_j$  of the initial field can be calculated by

$$P_j = \frac{1}{2^j} \sum_{l=0}^{2^j-1} (\tilde{\epsilon}^g_{j,l} - \langle \tilde{\epsilon}^g_{j,l} \rangle)^2, \tag{6}$$

where

$$\langle \tilde{\epsilon}_{j,l}^g \rangle = \frac{1}{2^j} \sum_{l=0}^{2^j - 1} \tilde{\epsilon}_{j,l}^g.$$

$$\tag{7}$$

In our numerical calculation, we generally use the compactly supported basis Daubechies 4 (D4) (Daubechies 1992). The choice of particular compactly supported wavelet basis does not effect the statistical results (Pando & Fang 1996) and the D4 wavelet is chosen as a matter of convenience. Although the so called Haar wavelet appears to be simpler, it is not well behaved in scale space (Fang & Thews 1998.)

#### 2.3. An example

To demonstrate the scale-by-scale Gaussian mapping, we recover the initial Gaussian mass field of a simulation sample of  $Ly\alpha$  forests.

The simulation samples are produced by a semi-analytic model of the intergalactic medium (Bi 1993; Fang et al. 1993.) This model approximately fits most observed features of the Ly $\alpha$  clouds, including the column density distribution and the number density of the lines, the distribution of equivalent widths and their redshift dependence, the clustering of the lines, and even the 3rd- and 4th-order non-Gaussian features (Bi, Ge & Fang 1995; Bi & Davidsen 1997, Feng & Fang, 2000.) We produce the simulation samples in redshift range  $z = 2.066 \sim 2.436$  with 2<sup>14</sup> pixels. The corresponding simulation size in the CDM model is 189.84 h<sup>-1</sup>Mpc in comoving space. These scales weakly depend on  $\Omega$ .

Figure 1 shows a typical realization of the simulated Ly $\alpha$ , including the flux F, density contrast of IGM,  $\delta_{IGM}$ , peculiar velocity of the IGM,  $V_{pec}$  and the column density of neutral hydrogen  $N_{HI}$ . The recovered IGM density distributions on scales  $10/2^j$  h<sup>-1</sup> Mpc and j = 6, 9, 12 are plotted in Fig. 2. These results show that the density distributions can be well reconstructed by the DWT algorithm. The small deviation of the recovered distributions from the original one is due mainly to the effect of the peculiar velocity. Figure 3 plots the DWT power spectra of the initial and recovered fields. It shows that the recovered power spectrum is in excellent agreement with the initial one until scale j = 9 or k = 10 h Mpc<sup>-1</sup>. This means that the effect of the peculiar velocity is significant only on small scales j > 9.

However, our goal is to put the scale-of-scale algorithm on a firm foundation and so recovering the power spectrum from simulation samples is insufficient for our purposes. We must investigate the conditions under which the basic assumption of the scale-of-scale algorithm – the order-preserving transformation – is reasonable.

#### 2.4. Conditions for quasi-locality

The scale-by-scale Gaussian mapping assumes the order preservation between the WFCs  $\tilde{\epsilon}_{j,l}$  of the evolved field and the initial WFCs  $\tilde{\epsilon}_{j,l}^0$  at each scale j. For scale j, index l corresponds to a spatial range  $L/2^j$ . The scale-by-scale Gaussianization algorithm does not require a point-point (or pixel-pixel) locality, but only a locality in the range of  $\Delta x = L/2^j$ .

For scale j, the corresponding wavenumber is  $k = 2\pi 2^j/L$  and we have

$$\Delta x \propto 2\pi/k. \tag{8}$$

That is, the size of the locality  $\Delta x$  in the scale-by-scale Gaussian mapping is scale-adaptive.

Only for wavelengths corresponding to one pixel is pixel-pixel locality required.

Obviously, if the locality condition is valid, the mode-mode correlation will be dominated by the local term. Thus, one can set a condition for the locality as

$$\frac{\langle \tilde{\epsilon}_{j,l} \tilde{\epsilon}_{j,l'} \rangle}{\langle \tilde{\epsilon}_{j,l}^2 \rangle} \ll 1, \quad l \neq l'.$$
(9)

For cosmological problems, the second order correlations  $\langle \tilde{\epsilon}_{j,l} \tilde{\epsilon}_{j,l'} \rangle$  only depend on the difference  $\Delta l = l' - l$ , and eq.(9) can be calculated as

$$\frac{\kappa_{j;j}(\Delta l)}{\kappa_{j;j}(0)} \ll 1, \quad \Delta l \neq 0, \tag{10}$$

where  $\kappa_{j;j,}(\Delta l)$  is defined by

$$\kappa_{j;j}(\Delta l) = \frac{1}{2^j} \sum_{l=0}^{2^j - 1} \tilde{\epsilon}_{j,l} \tilde{\epsilon}_{j,l+\Delta l}.$$
(11)

The ratios (10) or (11) can be used to estimate the error caused by the locality assumption.

#### 3. The evolution of the DWT modes in the Zel'dovich approximation

In this section, we will show that conditions eqs.(10) or (11) are reasonable in the weakly non-linear regime. We use the Zel'dovich solution, which describes the growing mode of the gravitational clustering in the quasi-linear and even non-linear regime until the variance of the density field is of order unity.

#### 3.1. The Zel'dovich solution in the DWT representation

In the Zel'dovich approximation [eq.(1)], the displacement vector field  $\mathbf{S}(\mathbf{q}, t)$  is given by

$$\mathbf{S}(\mathbf{q},t) = -b(t)\nabla\phi|_{\mathbf{q}},\tag{12}$$

where b(t) is the linear growth factor and  $\phi(\mathbf{q})$  is the initial irrotational peculiar velocity potential (Catelan 1995.) The Eulerian density field can be described as

$$\rho(\mathbf{x},t) = \bar{\rho}(t) \int d^3q \delta^D[\mathbf{x} - \mathbf{q} - \mathbf{S}(\mathbf{q},t)], \qquad (13)$$

where  $\delta^D(\mathbf{x})$  denotes the 3-dimensional Dirac delta function.

In the DWT representation, a density field  $\rho(\mathbf{x})$ ,  $\mathbf{x} = (x_1, x_2, x_3)$ , in range  $0 < x_i < L_i$ ,  $\{i = 1, 2, 3\}$  is described by the WFCs

$$\tilde{\epsilon}_{\mathbf{j},\mathbf{l}}(t) = \int \rho(\mathbf{x},t)\psi_{\mathbf{j},\mathbf{l}}(\mathbf{x})d\mathbf{x},\tag{14}$$

where the  $\psi_{\mathbf{j},\mathbf{l}}(\mathbf{x})$  are again an orthogonal and complete basis in 3-dimensions, constructed by the direct product of the 1-dimension wavelets (Daubechies 1992; Fang & Thews 1999)

$$\psi_{\mathbf{j},\mathbf{l}}(\mathbf{x}) = \psi_{j_1,l_1}(x_1)\psi_{j_2,l_2}(x_2)\psi_{j_3,l_3}(x_3).$$
(15)

Substituting eqs. (13) and (15) into eq.(14), we have

$$\tilde{\epsilon}_{\mathbf{j},\mathbf{l}}(t) = \int d^3 q \psi_{\mathbf{j},\mathbf{l}}[\mathbf{q} - b(t)\nabla\phi].$$
(16)

This is the solution of the DWT mode (j, l) evolution in the Zel'dovich approximation.

#### 3.2. Weakly non-linear evolution of the DWT modes

In the weakly non-linear regime, one can expand eq.(16) in a power series with respect to b(t)

$$\tilde{\epsilon}_{\mathbf{j},\mathbf{l}}(t) = \sum_{n=0}^{\infty} \frac{[-b(t)]^n}{n!} \int d^3 q (\nabla \phi \cdot \nabla)^n \psi_{\mathbf{j},\mathbf{l}}(\mathbf{q}).$$
(17)

The evolution of the DWT mode (j, l) can be calculated from the first few terms of eq.(17). Specifically, the first 4 terms give

1. The n = 0 term is

$$\tilde{\epsilon}_{\mathbf{j},\mathbf{l}}^{(0)}(t) = \int \psi_{\mathbf{j},\mathbf{l}}(\mathbf{q}) d^3 q = 0, \qquad (18)$$

where we used the admissibility property of wavelets. This is the uniform background.

2. The n = 1 term is

$$\tilde{\epsilon}_{\mathbf{j},\mathbf{l}}^{(1)}(t) = -b(t) \int d^3 q (\nabla \phi \cdot \nabla) \psi_{\mathbf{j},\mathbf{l}}(\mathbf{q}) = b(t) \int d^3 q \nabla^2 \phi \psi_{\mathbf{j},\mathbf{l}}(\mathbf{q})$$
(19)

Because  $\nabla^2 \phi$  is equal to the initial density contrast  $\delta_0(\mathbf{x})$ , we have

$$\tilde{\epsilon}_{\mathbf{j},\mathbf{l}}^{(1)}(t) = b(t) \int d^3q \delta_0(\mathbf{q}) \psi_{\mathbf{j},\mathbf{l}}(\mathbf{q}) = b(t) \tilde{\epsilon}_{\mathbf{j},\mathbf{l}}^0$$
(20)

where  $\tilde{\epsilon}_{\mathbf{j},\mathbf{l}}^0$  is given by

$$\tilde{\epsilon}_{\mathbf{j},\mathbf{l}}^{0} = \int d^{3}x \delta_{0}(\mathbf{x}) \psi_{\mathbf{j},\mathbf{l}}(\mathbf{x}).$$
(21)

Therefore,  $\tilde{\epsilon}_{\mathbf{j},\mathbf{l}}^0$  is the initial density perturbation of mode ( $\mathbf{j},\mathbf{l}$ ). Equation (20) gives the linear growth of mode ( $\mathbf{j},\mathbf{l}$ ) as b(t) is taken to be the growth solution of the density perturbations.

3. The n = 2 term is

$$\tilde{\epsilon}_{\mathbf{j},\mathbf{l}}^{(2)}(t) = \frac{b^2(t)}{2} \int d^3 q (\nabla \phi \cdot \nabla)^2 \psi_{\mathbf{j},\mathbf{l}}(\mathbf{q}) = -b^2(t) \int \nabla^2 \phi \nabla \phi \cdot \nabla \psi_{\mathbf{j},\mathbf{l}}(\mathbf{q}).$$
(22)

One can also decompose the initial velocity field  $\nabla \phi$  into the DWT modes (**j**, **l**) as

$$\tilde{\epsilon}_{\mathbf{j},\mathbf{l}}^{V_i} = \int d^3x \frac{\partial \phi}{\partial x_i} \psi_{j,l}(\mathbf{x}).$$
(23)

Thus, eq.(25) can be rewritten as

$$\tilde{\epsilon}_{\mathbf{j},\mathbf{l}}^{(2)}(t) = -b^2(t)\tilde{\epsilon}_{\mathbf{j}',\mathbf{l}'}^0 \tilde{\epsilon}_{\mathbf{j}'',\mathbf{l}''}^{V_i} \int d^3q \psi_{\mathbf{j}',\mathbf{l}'}(\mathbf{q})\psi_{\mathbf{j}'',\mathbf{l}''}(\mathbf{q})\frac{\partial}{\partial q_i}\psi_{\mathbf{j},\mathbf{l}}(\mathbf{q})$$
(24)

where the summation conventions for  $\mathbf{j}', \mathbf{l}', \mathbf{j}'', \mathbf{l}''$  and i are employed. Since the 3-dimensional wavelets are given by the direct product of 1-dimensional wavelets [eq.(15)], all terms in the r.h.s. of eq.(27) contain the three-wavelet integrals  $\int dx \psi_{j',l'}(x) \psi_{j'',l''}(x) \frac{d}{dx} \psi_{j,l}(x)$ . These integrals are non-zero only if the spatial ranges of the modes j', l' and j'', l'' overlap j, l. For the Daubechies 4 wavelet, l' and l'' should not differ from l by more than 2. Thus, this integral requires that (l, l', l'') be localized.

4. The n = 3 term is

$$\tilde{\epsilon}_{\mathbf{j},\mathbf{l}}^{(3)}(t) = -\frac{b^{3}(t)}{6} \int d^{3}q (\nabla \phi \cdot \nabla)^{3} \psi_{\mathbf{j},\mathbf{l}}(\mathbf{q}) \qquad (25)$$

$$= \frac{b^{3}(t)}{2} \tilde{\epsilon}_{\mathbf{j}',\mathbf{l}'}^{0} \tilde{\epsilon}_{\mathbf{j}'',\mathbf{l}''}^{V_{i}} \tilde{\epsilon}_{\mathbf{j}''',\mathbf{l}''}^{V_{k}} \int d^{3}q \psi_{\mathbf{j}',\mathbf{l}'}(\mathbf{q}) \psi_{\mathbf{j}'',\mathbf{l}''}(\mathbf{q}) \psi_{\mathbf{j}''',\mathbf{l}''}(\mathbf{q}) \frac{\partial}{\partial q_{i}} \frac{\partial}{\partial q_{k}} \psi_{\mathbf{j},\mathbf{l}}(\mathbf{q})$$

Similar to the 3-wavelet integral, the 4-wavelet integrals in eq.(25) require that the modes  $\mathbf{j}', \mathbf{l}', \mathbf{j}'', \mathbf{l}'', \mathbf{j}''', \mathbf{j}'''$  and  $\mathbf{j}, \mathbf{l}$  be localized.

Thus, the behavior of mode  $(\mathbf{j}, \mathbf{l})$  in the weak non-linear regime can be estimated as

$$\tilde{\epsilon}_{\mathbf{j},\mathbf{l}}(t) = \tilde{\epsilon}_{\mathbf{j},\mathbf{l}}^{(1)}(t) + \tilde{\epsilon}_{\mathbf{j},\mathbf{l}}^{(2)}(t) + \tilde{\epsilon}_{\mathbf{j},\mathbf{l}}^{(3)}(t).$$
(26)

Considering the locality of the wavelet integrals in eqs(24) and (25), eq.(26) yields

$$\tilde{\epsilon}_{\mathbf{j},\mathbf{l}}(t) \simeq b(t)\tilde{\epsilon}_{\mathbf{j},\mathbf{l}}^{0} \left[ 1 - b(t)\tilde{\epsilon}_{\mathbf{j}'',\mathbf{l}''}^{V_{i}} \int d^{3}q\psi_{\mathbf{j},\mathbf{l}}(\mathbf{q})\psi_{\mathbf{j}'',\mathbf{l}''}(\mathbf{q})\frac{\partial}{\partial q_{i}}\psi_{\mathbf{j},\mathbf{l}}(\mathbf{q}) + \frac{b^{2}(t)}{2}\tilde{\epsilon}_{\mathbf{j}'',\mathbf{l}''}^{V_{i}}\tilde{\epsilon}_{\mathbf{j}''',\mathbf{l}''}^{V_{k}} \int d^{3}q\psi_{\mathbf{j},\mathbf{l}}(\mathbf{q})\psi_{\mathbf{j}'',\mathbf{l}''}(\mathbf{q})\psi_{\mathbf{j}''',\mathbf{l}''}(\mathbf{q})\frac{\partial}{\partial q_{i}}\frac{\partial}{\partial q_{k}}\psi_{\mathbf{j},\mathbf{l}}(\mathbf{q})\right]$$

$$(27)$$

If the initial density and velocity perturbations are Gaussian, we have

$$\langle \tilde{\epsilon}_{\mathbf{j},\mathbf{l}}^{0} \rangle = \langle \tilde{\epsilon}_{\mathbf{j},\mathbf{l}}^{V_{i}} \rangle = 0$$

$$\langle \tilde{\epsilon}_{\mathbf{j}',\mathbf{l}'}^{V_{i}} \tilde{\epsilon}_{\mathbf{j}'',\mathbf{l}''}^{0} \rangle = 0$$

$$(28)$$

and

$$\langle \tilde{\epsilon}^{0}_{\mathbf{j}',\mathbf{l}'} \tilde{\epsilon}^{0}_{\mathbf{j}'',\mathbf{l}''} \rangle = \langle \tilde{\epsilon}^{V_{i}}_{\mathbf{j}'',\mathbf{l}''} \tilde{\epsilon}^{V_{k}}_{\mathbf{j}''',\mathbf{l}''} \rangle = 0,$$

$$\text{if } \mathbf{j}' \neq \mathbf{j}'' \text{ or } \mathbf{l}' \neq \mathbf{l}''.$$

$$(29)$$

All high order cumulants of  $\tilde{\epsilon}^{0}_{\mathbf{i}',\mathbf{l}'}$  and  $\tilde{\epsilon}^{V_{i}}_{\mathbf{i}',\mathbf{l}'}$  are also zero.

Thus, in the bracketed expression of the r.h.s. of eq.(27), the second term is zero on average because the initial Gaussian velocity perturbations  $\langle \tilde{\epsilon}_{\mathbf{j}'',\mathbf{l}''}^{V_i} \rangle = 0$ . The third term in the bracket is proportional to the variance of  $\tilde{\epsilon}_{\mathbf{j},\mathbf{l}}^{V_i}$ , and then to the variance of  $\tilde{\epsilon}_{\mathbf{j},\mathbf{l}}^0$ . Therefore, large initial WFCs  $\tilde{\epsilon}_{\mathbf{j},\mathbf{l}}^0$  statistically evolve into large  $\tilde{\epsilon}_{\mathbf{j},\mathbf{l}}(t)$ , and low initial WFCs into low WFCs. The evolution is monotonic.

#### 3.3. Quasi-locality of second order correlations in phase space

The locality can be expressed by the mode-mode correlations. For the second order correlation between modes  $(\mathbf{j^1}, \mathbf{l^1})$  and  $(\mathbf{j^2}, \mathbf{l^2})$ , the non-zero terms up to order  $b^4$  are

$$\begin{split} \langle \tilde{\epsilon}_{\mathbf{j}\mathbf{l},\mathbf{l}\mathbf{l}}(t) \tilde{\epsilon}_{\mathbf{j}\mathbf{2},\mathbf{l}\mathbf{2}}(t) \rangle &= \qquad (30) \\ &= \langle \tilde{\epsilon}_{\mathbf{j}\mathbf{l},\mathbf{l}\mathbf{l}}^{(1)}(t) \tilde{\epsilon}_{\mathbf{j}\mathbf{2},\mathbf{l}\mathbf{2}}^{(1)}(t) \rangle + \langle \tilde{\epsilon}_{\mathbf{j}\mathbf{l},\mathbf{l}\mathbf{l}}^{(2)}(t) \tilde{\epsilon}_{\mathbf{j}\mathbf{2},\mathbf{l}\mathbf{2}}^{(2)}(t) \rangle + \langle \tilde{\epsilon}_{\mathbf{j}\mathbf{1},\mathbf{l}\mathbf{l}}^{(1)}(t) \tilde{\epsilon}_{\mathbf{j}\mathbf{2},\mathbf{l}\mathbf{2}}^{(3)}(t) \rangle + \langle \tilde{\epsilon}_{\mathbf{j}\mathbf{1},\mathbf{l}\mathbf{l}}^{(1)}(t) \tilde{\epsilon}_{\mathbf{j}\mathbf{2},\mathbf{l}\mathbf{2}}^{(1)}(t) \rangle \\ &= b^{2}(t) \langle \tilde{\epsilon}_{\mathbf{j}\mathbf{1},\mathbf{l}\mathbf{1}}^{0} \tilde{\epsilon}_{\mathbf{j}\mathbf{2},\mathbf{l}\mathbf{2}}^{0} \rangle + b^{4}(t) \langle \tilde{\epsilon}_{\mathbf{j}\mathbf{1},\mathbf{l}}^{0} \tilde{\epsilon}_{\mathbf{j}\mathbf{1},\mathbf{l}^{\prime}}^{V_{i}} \tilde{\epsilon}_{\mathbf{j}^{\prime\prime\prime},\mathbf{l}^{\prime\prime\prime\prime}}^{V_{k}} \tilde{\epsilon}_{\mathbf{j}^{\prime\prime\prime\prime},\mathbf{l}^{\prime\prime\prime\prime}}^{V_{k}} \rangle \times \\ &\int d^{3}q\psi_{\mathbf{j},\mathbf{l}}(\mathbf{q})\psi_{\mathbf{j}^{\prime\prime\prime},\mathbf{l}^{\prime\prime\prime}}(\mathbf{q}) \frac{\partial}{\partial q_{i}}\psi_{\mathbf{j}\mathbf{1},\mathbf{l}\mathbf{1}}(\mathbf{q}) \int d^{3}q\psi_{\mathbf{j}^{\prime},\mathbf{l}^{\prime\prime}}(\mathbf{q})\psi_{\mathbf{j}^{\prime\prime\prime\prime},\mathbf{l}^{\prime\prime\prime\prime}}(\mathbf{q}) \frac{\partial}{\partial q_{i}}\psi_{\mathbf{j}\mathbf{2},\mathbf{l}\mathbf{2}}(\mathbf{q}) \\ &+ \frac{b^{4}(t)}{2} \left\{ \langle \tilde{\epsilon}_{\mathbf{j}\mathbf{1},\mathbf{l}\mathbf{1}}^{0} \tilde{\epsilon}_{\mathbf{j}^{\prime\prime},\mathbf{l}^{\prime\prime}}^{V_{k}} \tilde{\epsilon}_{\mathbf{j}^{\prime\prime\prime\prime},\mathbf{l}^{\prime\prime\prime\prime}}^{V_{k}} \rangle \int d^{3}q\psi_{\mathbf{j}^{\prime},\mathbf{l}^{\prime\prime}}(\mathbf{q})\psi_{\mathbf{j}^{\prime\prime\prime\prime},\mathbf{l}^{\prime\prime\prime\prime}}(\mathbf{q}) \frac{\partial}{\partial q_{i}}\frac{\partial}{\partial q_{k}}\psi_{\mathbf{j}\mathbf{2},\mathbf{l}\mathbf{2}}(\mathbf{q}) \\ &+ [(\mathbf{j}\mathbf{1},\mathbf{l}\mathbf{1}) \rightleftharpoons (\mathbf{j}^{2},\mathbf{l}^{2})] \right\}. \end{split}$$

The term  $b^2(t)$  is the linear term and the  $b^4(t)$  term gives the first non-linear correction.

Due to the locality of the 3- and 4-wavelet integrals, eq.(30) yields

$$\langle \tilde{\epsilon}_{\mathbf{j}^1,\mathbf{l}^1}(t)\tilde{\epsilon}_{\mathbf{j}^2,\mathbf{l}^2}(t)\rangle \simeq 0.$$
 (31)

The second order correlations between the DWT modes  $(\mathbf{j}, \mathbf{l})$  are localized [eqs.(9) and (10)].

Since the 3- and 4-wavelet integrals do not require that scales  $\mathbf{j}$  be the same as  $\mathbf{j}'$ ,  $\mathbf{j}''$ , and  $\mathbf{j}'''$ , there exist correlations between modes on different scales but localized in the same spatial range. That is

$$\langle \tilde{\epsilon}_{\mathbf{j}^1,\mathbf{l}^1} \tilde{\epsilon}_{\mathbf{j}^2,\mathbf{l}^1} \rangle \neq 0.$$
 (32)

This second order correlation actually is a non-Gaussian correlation which corresponds to the non-random phase of the Fourier modes, or the phase-phase correlations between the Fourier modes (Feng & Fang 2000)

Moreover, the spatial size of a mode on scale j is  $L/2^{j}$ . Thus, the scale-scale correlations between j' and j lead to a dependence of perturbations at  $L/2^{j'}$  on the perturbations at  $L/2^{j}$ . The two perturbations are not perfectly localized in the same area, and therefore, the coupling between the DWT modes is quasi-local. In the fully developed non-linear regime, the strong scale-scale correlations will finally lead to non-local correlations of the DWT modes.

## 3.4. Non-Gaussianity of third-order correlations

The non-Gaussianities on higher-order correlations caused by the weakly non-linear evolution can be calculated by the cumulants of  $\tilde{\epsilon}_{\mathbf{j},\mathbf{l}}$ . Using eq.(29), the third order correlation up to order  $b^4$  is

$$\langle \tilde{\epsilon}_{\mathbf{j}^{1},\mathbf{l}^{1}}\tilde{\epsilon}_{\mathbf{j}^{2},\mathbf{l}^{2}}\tilde{\epsilon}_{\mathbf{j}^{3},\mathbf{l}^{3}} \rangle = \langle \tilde{\epsilon}_{\mathbf{j}^{1},\mathbf{l}^{1}}^{(1)}(t)\tilde{\epsilon}_{\mathbf{j}^{2},\mathbf{l}^{2}}^{(1)}(t)\tilde{\epsilon}_{\mathbf{j}^{3},\mathbf{l}^{3}}^{(1)}(t) \rangle + [\langle \tilde{\epsilon}_{\mathbf{j}^{1},\mathbf{l}^{1}}^{(1)}(t)\tilde{\epsilon}_{\mathbf{j}^{2},\mathbf{l}^{2}}^{(1)}(t)\tilde{\epsilon}_{\mathbf{j}^{3},\mathbf{l}^{3}}^{(2)}(t) \rangle + 2 \text{ terms with cyc. permutations].}$$

$$(33)$$

For Gaussian initial perturbation eq.(28), we have

$$\langle \tilde{\epsilon}_{\mathbf{j}^{1},\mathbf{l}^{1}}^{(1)}(t)\tilde{\epsilon}_{\mathbf{j}^{2},\mathbf{l}^{2}}^{(1)}(t)\tilde{\epsilon}_{\mathbf{j}^{3},\mathbf{l}^{3}}^{(1)}(t)\rangle \propto \langle \tilde{\epsilon}_{\mathbf{j}^{1},\mathbf{l}^{1}}^{0}(t)\tilde{\epsilon}_{\mathbf{j}^{2},\mathbf{l}^{2}}^{0}(t)\tilde{\epsilon}_{\mathbf{j}^{3},\mathbf{l}^{3}}^{0}(t)\rangle = 0.$$
(34)

Using eq.(24) we have

$$\langle \tilde{\epsilon}_{\mathbf{j}\mathbf{l},\mathbf{l}\mathbf{l}}^{(1)}(t) \tilde{\epsilon}_{\mathbf{j}\mathbf{2},\mathbf{l}\mathbf{2}}^{(2)}(t) \tilde{\epsilon}_{\mathbf{j}\mathbf{3},\mathbf{l}\mathbf{3}}^{(2)}(t) \rangle \propto$$

$$\langle \tilde{\epsilon}_{\mathbf{j}\mathbf{l},\mathbf{l}\mathbf{l}}^{0}(t) \tilde{\epsilon}_{\mathbf{j}\mathbf{2},\mathbf{l}\mathbf{2}}^{0}(t) \rangle \tilde{\epsilon}_{\mathbf{j}',\mathbf{l}'}^{0} \tilde{\epsilon}_{\mathbf{j}'',\mathbf{l}''}^{V_{i}} \rangle \int d^{3}q \psi_{\mathbf{j}',\mathbf{l}'}(\mathbf{q}) \psi_{\mathbf{j}'',\mathbf{l}''}(\mathbf{q}) \frac{\partial}{\partial q_{i}} \psi_{\mathbf{j}\mathbf{3},\mathbf{l}\mathbf{3}}(\mathbf{q}) = 0.$$

$$(35)$$

Therefore, the largest two terms of eq.(33) are zero and we have

$$\langle \tilde{\epsilon}_{\mathbf{j}^1,\mathbf{l}^1} \tilde{\epsilon}_{\mathbf{j}^2,\mathbf{l}^2} \tilde{\epsilon}_{\mathbf{j}^3,\mathbf{l}^3} \rangle \simeq 0.$$
 (36)

That is, the one-point distribution of the DWT modes  $(\mathbf{j}, \mathbf{l})$  contains at most a small skewness.

This result can also be obtained from the hierarchical clustering or linked-pair approximation as

$$\langle \delta(\mathbf{x}^1) \delta(\mathbf{x}^2) \delta(\mathbf{x}^3) \rangle \simeq Q_3[\langle \delta(\mathbf{x}^1) \delta(\mathbf{x}^2) \rangle \langle \delta(\mathbf{x}^1) \delta(\mathbf{x}^3) \rangle$$

$$+ 2 \text{ terms with cyc. permutations]},$$

$$(37)$$

where  $\delta(\mathbf{x}) = [\rho(\mathbf{x}) - \bar{\rho}]/\bar{\rho}$ . Since wavelet  $\psi_{j,l}$  is admissible, i.e.,  $\int \psi_{j,l}(x) dx = 0$ , eq.(17) gives

$$\tilde{\epsilon}_{\mathbf{j},\mathbf{l}}(t) = \frac{1}{\bar{\rho}} \int \delta(\mathbf{x}) \psi_{\mathbf{j},\mathbf{l}}(\mathbf{x}) d\mathbf{x}.$$
(38)

We can take  $\bar{\rho} = 1$ , i.e., the mean density is normalized.

Expressing eq.(38) in the wavelet basis  $\psi_{\mathbf{j},\mathbf{l}^1}(\mathbf{x}^1)\psi_{\mathbf{j}^2,\mathbf{l}^2}(\mathbf{x}^2)\psi_{\mathbf{j}^3,\mathbf{l}^3}(\mathbf{x}^3)$ , we have

$$\langle \tilde{\epsilon}_{\mathbf{j},\mathbf{l}^{1}} \tilde{\epsilon}_{\mathbf{j},\mathbf{l}^{2}} \tilde{\epsilon}_{\mathbf{j},\mathbf{l}^{3}} \rangle \simeq Q_{3} \sum_{\mathbf{l}',\mathbf{l}''} a_{\mathbf{l}^{1},\mathbf{l}'^{1},\mathbf{l}''^{1}}^{3} [\langle \tilde{\epsilon}_{\mathbf{j},\mathbf{l}'^{1}} \tilde{\epsilon}_{\mathbf{j},\mathbf{l}^{2}} \rangle \langle \tilde{\epsilon}_{\mathbf{j},\mathbf{l}''^{1}} \tilde{\epsilon}_{\mathbf{j},\mathbf{l}^{3}} \rangle$$
(39)

+ 3 terms with cyc. permutations].

where  $a^3_{\mathbf{l}^1,\mathbf{l}'^1,\mathbf{l}''^1}$  is given by the 3-wavelet integral,

$$a_{\mathbf{l}^{1},\mathbf{l}^{\prime 1},\mathbf{l}^{\prime \prime 1}}^{3} = \int \psi_{\mathbf{j},\mathbf{l}^{1}}(\mathbf{x})\psi_{\mathbf{j},\mathbf{l}^{\prime 1}}(\mathbf{x})\psi_{\mathbf{j},\mathbf{l}^{\prime \prime 1}}(\mathbf{x})d\mathbf{x}.$$
(40)

 $a_{l^1,l'^1,l''1}^3$  generally is small and exactly equal to zero for the Haar wavelets (Mallat 1989a; Meyer 1992). Therefore, a hierarchical clustered field is only weakly skewed. Note however, that this does *not* imply that the skewness in the DWT representation is small in general.

### 3.5. Non-Gaussianity of fourth-order correlations

In contrast, the 4th-order correlations of the WFCs given by eq.(26) are generally nonzero at order  $b^4$ . The first significant non-zero higher order term not caused by  $\rho \ge 0$  is the kurtosis defined by

$$K_{j} = \frac{\langle (\tilde{\epsilon}_{\mathbf{j},\mathbf{l}} - \langle \tilde{\epsilon}_{\mathbf{j},\mathbf{l}} \rangle)^{4} \rangle}{\langle \tilde{\epsilon}_{\mathbf{j},\mathbf{l}}^{2} \rangle^{2}} - 3.$$

$$(41)$$

The kurtosis can be considered as a special case  $(j = j' \text{ and } \Delta l = 0)$  of the fourth order scale-scale correlations defined by

$$C_{j,j'}^{2,2}(\Delta l) = \frac{2^{j'} \sum_{l=0}^{2^{j'-1}} \tilde{\epsilon}_{j;[l/2^{j'-j}]+\Delta l}^2 \tilde{\epsilon}_{j';l}^2}{\sum \tilde{\epsilon}_{j,[l/2^{j'-j}]}^2 \sum \tilde{\epsilon}_{j';l}^2}.$$
(42)

 $C_{j;j'}^{2,2}(\Delta l)$  measures the correlations between the perturbations of modes on scales j and j', at two positions separated a distance  $\Delta lL/2^{j}$ . In the case of  $\Delta l = 0$ ,  $C_{j;j'}^{2,2}(0)$  measures the correlation between fluctuations on scale j and j' at the *same* physical point.

Using the locality of the 4-wavelet integral in eq.(25), one can show that the scale-scale correlations in the weakly non-linear regime are also localized, i.e.,

$$C_{j;j'}^{2,2}(\Delta l \neq 0) \ll C_{j;j'}^{2,2}(0).$$
 (43)

In the weakly non-linear regime, the phase space behavior of gravitational clustering for an initially Gaussian mass field can be summarized as

- 1. The evolution is spatially quasi-localized, i.e., the correlations between WFCs at different positions are always less than that at the same position.
- 2. The density field contains a very small skewness.
- 3. The major non-Gaussianities are local scale-scale correlations.

It should be pointed out that if a distribution possesses the above-listed features, it does not mean that the initial mass field is Gaussian. Actually, for a distribution to exhibit these features, we only need the following conditions on the initial density perturbation:

$$\langle \tilde{\epsilon}^0_{\mathbf{j},\mathbf{l}} \tilde{\epsilon}^0_{\mathbf{j}',\mathbf{l}'} \rangle = 0, \tag{44}$$

when the spatial range of l doesn't overlap l', and

$$\langle \tilde{\epsilon}_{\mathbf{j},\mathbf{l}}^{0} \tilde{\epsilon}_{\mathbf{j}',\mathbf{l}'}^{0} \rangle \neq 0, \tag{45}$$

when the spatial range of l does overlap l'. The conditions given by eqs.(44) and (45) are weaker than eqs.(28) and (29). The initial field given by eqs.(44) and (45) can be non-Gaussian.

Equations (44) and (45) show once again that the statistical properties of a random field should be described by two types of correlations: one with respect to scale j and the other with respect to position l. These two types of correlations correspond to correlations with respect to the phase and amplitude in the Fourier representation. It is, in fact, possible to construct clustering models which lead to a density field with a Poisson or Gaussian PDF with respect to l, but that are highly scale-scale correlated (Greiner, Lipa & Carruthers, 1995.)

## 3.6. Redshift space

If the density field is viewed in redshift space, the observed radial position is given by the radial velocity consisting of the uniform Hubble flow and the peculiar motion  $\mathbf{v}(\mathbf{x})$ . Thus the position  $\mathbf{x}$  in eq.(1) should be replaced by

$$\mathbf{s} = \mathbf{x} + [\hat{\mathbf{z}} \cdot \mathbf{v}(\mathbf{x})]\hat{\mathbf{z}},\tag{46}$$

where  $\hat{\mathbf{z}}$  is taken to be in the direction of the line of sight. The second term in eq.(46) is the correction due to the radial peculiar velocity.

In redshift space the Zel'dovich solution eq.(16) is replaced by (e.g. Taylor & Hamilton 1996)

$$\rho(\mathbf{s},t) = \bar{\rho}(t) \int d^3q \delta^D[\mathbf{s} - \mathbf{q} - \mathbf{S}^{\mathbf{s}}(\mathbf{q},t)].$$
(47)

In the linear approximation of the velocity field, the displacement vector field is

$$\mathbf{S}^{\mathbf{s}}(\mathbf{q}) = \mathbf{S}(\mathbf{q}) + \Omega^{0.6}[\hat{\mathbf{z}} \cdot \mathbf{S}(\mathbf{x})]\hat{\mathbf{z}}, \qquad (48)$$

where  $\Omega$  is the cosmological density parameter. Thus, the solution [eq.(19)] becomes

$$\tilde{\epsilon}_{\mathbf{j},\mathbf{l}}(t) = \int d^3 q \psi_{\mathbf{j},\mathbf{l}}[\mathbf{q} + \mathbf{S}^{\mathbf{s}}(\mathbf{q},t)].$$
(49)

This is the Zel'dovich solution for the DWT modes in redshift space. Mathematically, eq.(48) is equivalent to eq.(16), with  $\mathbf{S}^{s}(\mathbf{q}, t)$  replacing  $\mathbf{S}(\mathbf{q}, t)$ . Therefore, all results drawn from eq.(16) still hold for eq.(49) if the intersection of the particle trajectories has not yet happen.

It is known that the non-linear effect of the redshift distortion, like the Fingers-of-God in the galaxy distribution in redshift space, cannot be modeled by the Zel'dovich solution. In other words, the non-linear effects of the redshift distortion are not negligible if the Zel'dovich solution fails. Thus, the scale on which the quasi-locality assumption is no longer correct is also the scale where the non-linear redshift distortion effects emerge. This result is consistent with the numerical example shown in §2.3, which shows that on scales as small as j = 9, the scale-by-scale reconstruction is still very good, and the redshift distortion effects are not yet significant.

#### 4. Quasi-locality in the Ly $\alpha$ forests

To test the predictions on the quasi-locality of the DWT mode-mode correlations (§3.5), we analyze samples of the QSO  $Ly\alpha$  absorption spectrum which are believed to trace the

underlying mass field in the weakly non-linear regime. The second point listed in §3.5 has been tested by our previous studies, which showed no skewness above a positive definite random distribution for the distributions of Ly $\alpha$  forests lines (Pando & Fang 1998a) or the transmitted flux (Feng & Fang 2000.) In this section, we will focus on the points 1 and 3.

The QSO Ly $\alpha$  absorption spectrum samples used in our analysis are: 1.) the transmitted flux of HS1700+64 Ly $\alpha$  absorptions; 2.) the Ly $\alpha$  forest lines from moderate resolution spectrum, including a sample compiled by Lu, Wolfe, & Turnshek (LWT) (1991) that contains ~ 950 lines from the spectra of 38 QSOs, and a sample compiled by Bechtold (JB) (1994) which contains a total ~ 2800 lines from 78 QSO's spectra in which 34 high-redshift QSO's were observed, and 3.) the Ly $\alpha$  forest lines from high resolution spectrum, including the data of Hu et al. (HU) (1995) which has ~ 1056 lines from four quasars in wavelength range 4300-5100 Å measured with the HIRES spectrograph on the Keck, and the HIRES data of QSO HS1946+7658 of Kirkman & Tytler (HT) (1997).

The simulation samples used in this section are the same ones used in  $\S2.3$ .

# 4.1. Quasi-locality of the second order DWT mode-mode correlation

Figure 4 shows  $\kappa_{j,j}(\Delta l)$  for 100 realizations of the simulated Ly $\alpha$  transmitted flux and QSO HS1700+64. Here we use the Daubechies 4 wavelets in our calculations as these wavelets are better behaved in scale space. Figure 4 shows clearly that the condition for locality eq.(13) holds. The correlations  $\kappa_{j,j}(\Delta l)$  for all  $\Delta l \neq 0$  are sharply lower than  $\kappa_{j,j}(0)$ . For small scales j > 5, at the 95% confidence level, the non-local correlations are no more than 20%.

Figure 5 shows the correlation  $\kappa_{j,j+1}(\Delta l)$ , the second order correlations between scales j and j + 1. Comparing with  $\kappa_{j,j}(0)$ , the second order non-local scale-scale correlations  $(\Delta l \neq 0)$  show no power. For the local case,  $\kappa_{j,j+1}(0)$  generally also has no power. But it is interesting to note that  $\kappa_{j,j+1}(0)$  becomes significant on very small scales j = 9, 10. This is a second order non-Gaussian detection. One can similarly detect other second order scale-scale correlations, such (j, j + 2), (j, j + 3) etc. with similar results.

Figures 6 and 7 are similar to Fig. 4 but for the LWT/JB and HU/KT Ly $\alpha$  forest line samples. Although the identification of absorption lines from transmitted flux may introduce an arbitrary bias, the LWT/JB and HU/KT data show the same behavior as  $\kappa_{j,j}(\Delta l)$  in Fig. 4. For scales j > 5, the locality eq. (10) is a very good approximation, even considering the large error in the data. For each QSO, we calculate the statistical quantity  $\kappa_{j,j+1}(\Delta l)$ , and the mean and 1- $\sigma$  error bars are found from the ensemble of these QSOs. Since there are more QSO's in the LWT/JB data, the error bars for the LWT/JB data are smaller than the high resolution data HU/KT.

Figures 8 and 9 are similar to Fig. 5 but again for the  $Ly\alpha$  forest lines. The results once again show that the behavior of the second order scale-scale correlations for the forest line samples is the same as the transmitted flux samples. There is no power in these second order scale-scale correlations.

## 4.2. Quasi-locality of 4th order non-Gaussianity

In the previous section, we detected the local scale-scale correlation from the second order statistics. The local correlation of the 4th-order statistics is more prominent. In our previous studies, we have shown that the Ly $\alpha$  forests are significantly non-Gaussian at 4thorder, including the kurtosis (Pando & Fang 1998a) and the scale-scale correlations (Pando et al. 1998, Feng & Fang 2000). In this section, we will show that although the 4th-order local correlations are strong, the non-local correlations are weak.

The 4th-order statistic in Figure 10 is defined by

$$Q_{j}^{2,2}(\Delta l) = \frac{2^{j} \sum_{l=0}^{2^{j}-1} \tilde{\epsilon}_{j;l}^{2} \tilde{\epsilon}_{j;l+\Delta l}^{2}}{\sum \tilde{\epsilon}_{j;l}^{2} \sum \tilde{\epsilon}_{j;l+\Delta l}^{2}}.$$
(50)

For the local case, i.e.,  $\Delta l = 0$ ,  $Q_j^{2,2}(0)$  is the compact form of the kurtosis

$$K_{j} = \frac{2^{j} \sum_{l=0}^{2^{j}-1} \tilde{\epsilon}_{j;l}^{4}}{[\sum_{l=0}^{2^{j}-1} \tilde{\epsilon}_{j,l}^{2}]^{2}}.$$
(51)

Figure 10 shows that the non-local correlation  $Q_j^{2,2}(\Delta l)$  with  $\Delta l \neq 0$  of the transmitted flux generally is around 1, i.e., no correlation. On small scales  $j \geq 5$  the local correlation  $Q_j^{2,2}(0)$  gradually becomes significant, while the non-local correlation  $Q_j^{2,2}(\Delta l)$  with  $\Delta l \neq 0$ still remains at 1. This result supports the quasi-locality condition.

Figure 11 displays  $C_j^{2,2}(\Delta l)$ , which is the scale-scale correlation between scales j and j + 1, and shows that the non-local scale-scale correlation  $C_j^{2,2}(\Delta l)$  with  $\Delta l \neq 0$  generally is around 1, i.e., no correlation. When the local scale-scale correlation becomes significant on scales  $j \geq 7$ , the non-local correlation  $C_j^{2,2}(\Delta l)$  with  $\Delta l \neq 0$  still remains at 1.

Unlike the second order scale-scale correlations, the 4th-order correlations  $Q_j^{2,2}(0)$  and  $C_j^{2,2}(0)$  are significant. There is substantial power on all scales  $j \ge 5$ .

Figures 12 and 13 show the scale-scale correlations for the LWT/JB and HU/KT Ly $\alpha$  forest lines, respectively. Figure 9 clearly shows a steady decrease in the scale-scale amplitudes with  $\Delta l$ . This again demonstrates the quasi-locality. Fig. 10 also shows a decrease in the scale-scale amplitudes with  $\Delta l$ , but it is rather slow. Even when  $\Delta l = 3$ , the correlation remains. These non-local correlations may be caused by problems in identifying the lines, and if so, indicates that the transmitted flux is better suited than the Ly $\alpha$  forest lines for a Gaussianization reconstruction.

### 5. Conclusions and discussions

In this work we have demonstrated that the assumptions necessary for reconstructing an initial density field by a scale-dependent Gaussianization procedure are justified. The assumptions, namely the locality and monotonic nature of the gravitational clustering, are borne out by both the Zel'dovich approximation and correlation analysis of QSO Ly $\alpha$  samples. That is, the DWT mode-mode coupling caused by the weakly non-linear evolution of the gravitational clustering is quasi-local and that the large initial WFCs evolve into large WFCs of the observed density field. This result provides a solid basis for the DWT scale-by-scale Gaussianization reconstruction of Ly $\alpha$  forests.

The non-Gaussianities produced by the mode-mode coupling during the weakly nonlinear regime are mainly local scale-scale correlations. This result explains why the Gaussianization reconstruction is substantially improved by removing the local scale-scale correlations (Feng & Fang 2000.) Clearing the local scale-scale correlation is a key for an effective Gaussianization reconstruction. All these features provide a solid basis for the DWT scaleby-scale (or scale-adaptive) Gaussianization reconstruction algorithm.

Since galaxies undergo a highly non-linear evolution, and their bias might be nonmonotonic, the validity of the order preserving assumption for the galaxy field needs further study. Whether a sample is suitable for the DWT scale-by-scale reconstruction can be judged by detecting the non-local mode-mode correlations. If the scale-scale correlations are significantly non-local, the sample will not be a good candidate for a DWT scale-byscale Gaussianization. The local scale-scale correlation have been detected in recent years for galaxy samples, such as the APM bright galaxy catalog (Feng, Deng & Fang 2000.) However, it remains to be determined whether these couplings are non-localized.

In essence, the DWT analysis looks at the phase space behavior of the gravitational clustering. While there are many perturbation calculations of the clustering dynamics in the Fourier and coordinate representations (Buchert 1993; Bouchet et al. 1995; Catelan 1995),

the locality cannot be revealed with these calculations, because in the Fourier representation, the phases hold the position information (locality) of the relevant Fourier modes. This makes it practically impossible to determine the locality of clustering in the Fourier representation. The DWT analysis may also be useful in studying other clustering features in the Zel'dovich approximation for which a phase space description is essential, such as the breakdown of the Galilean invariance or the lack of momentum conservation (Polyakov 1995; Scoccimarro 1998.)

This work was supported in part by the LWL foundation. We thank Dr. D. Tytler for kindly providing the data of the Keck spectrum HS1700+64. LLF acknowledges support from the National Science Foundation of China (NSFC) and World Laboratory Scholarship.

## REFERENCES

- Adler, R.J. 1981, The Geometry of Random Fields, (Wiley, New York)
- Bechtold, J., 1994, ApJS, 91,1.
- Bi. H. G. 1993, ApJ, 405, 479
- Bi, H.G & Davidson, A. F., 1997, ApJ, 479, 523.
- Bi, H.G., Ge, J. & Fang, L.Z. 1995, ApJ, 452, 90
- Bouchet, F., Colombi, S., Hivon, E., & Juszkiewicz, R., 1995 A&A, 296, 575
- Buchert, T., 1993, A&A, 267, L51.
- Catelan, P. 1995, MNRAS, 276, 115
- Croft, R.A.C., Weinberg, D.H., Katz, N. & Hernquist, L. 1998, ApJ, 495, 44
- Croft, R.A.C., Weinberg, Pettini, M. D.H., Hernquist, L. & Katz, N. 1999, ApJ, 520, 1
- Daubechies I. 1992, Ten Lectures on Wavelets, (Philadelphia, SIAM)
- Fang, L.Z., Bi, H.G., Xiang, S.P. & Börner, G. 1993, ApJ, 413, 477
- Fang, L.Z. & Thews, R. 1998, Wavelets in Physics, (World Scientific, Singapore)
- Feng, L.L., Deng, Z.G. & Fang, L.Z. 2000, ApJ, 530, 53
- Feng, L.L., & Fang, L.Z. 2000, ApJ, 535, 519
- Greiner, M., Lipa, P. & Carruthers, P. 1995, Phys. Rev. E51, 1948
- Hernquist, L., Katz, N., Weinberg, D.H. & Miralda-Escudé, J. 1996, ApJ, 457, L5
- Hu, E.M., Kim, T.S., Cowie, L.L., Songaila, A., Rauch, M., 1995, AJ, 110, 1526.

- Hui, L., Gnedin, N. & Zhang, Y. 1997, ApJ, 486, 599
- Kirkman, D., Tytler, D., 1997, ApJ, 484, 672.
- Lu, L., Wolfe, A.M., & Turnshek, D.A., 1991, ApJ, 367, 19.
- Mallat, S.G. 1989a, IEEE Trans, on PAMI, 11, 674
- Mallat, S.G. 1989b, Trans. Am. Math. Soc. 315, 69
- Meyer, Y. 1992, Wavelets and Operators, (Cambridge Press, New York).
- Monaco, P. & Efstathiou, G. 2000, MNRAS, 308, 763
- Narayanan, V. & Weinberg, D. 1998, ApJ, 508, 440
- Pando, J. & Fang, L.Z. 1996, ApJ, 459, 1
- Pando, J. & Fang, L.Z. 1998a, A&A, 340, 335
- Pando, J. & Fang, L.Z. 1998b, Phys. Rev. E57, 3593
- Pando, J., Greiner, M., Lipa, P. & Fang, L.Z., 1998, ApJ, 496, 9
- Peebles, P.J.E. 1980, The Large Scale Structure of the Universe, Princeton Univ. Press
- Polyakov, A.M. 1995, Phys. Rev. E52 6183
- Scoccimarro, R. 1998, MNRAS, 299, 1097
- Suto, Y. & Sasaki, M. 1991, Phys. Rev. Lett. 66, 264
- Taylor, A.N. & Hamilton, A. 1996, MNRAS, 282, 767
- Vanmarke, E.H. 1983, Random Fields, (MIT Press)
- Weinberg, D.H. 1992, MNRAS, 254, 315
- Xu, W., Fang, L.Z. & Wu, X.P. 2000, ApJ, in press
- Zel'dovich, Ya.B. 1970, A & A, 5, 84

This preprint was prepared with the AAS  ${\tt IAT}_{\rm E\!X}$  macros v5.0.

Fig. 1.— A simulated sample of the Ly $\alpha$  forest, including the flux F, the IGM density contrast  $\delta_{IGM}$ , peculiar velocity  $V_{pec}$  and column density of neutral hydrogen  $N_{HI}$ .

Fig. 2.— The IGM density field (left panel) and flux (right panel). The solid lines are for the reconstructed density field and flux by the scale-by-scale Gaussianization. The dotted lines are the original fields.

Fig. 3.— The DWT power spectra of the mass fields recovered by the scale-by-scale algorithm. The error bars are the  $1\sigma$  deviation calculated for the 100 realizations.

Fig. 4.— The dependence of  $\kappa_{j,j}(\Delta l)$  on  $\Delta l$ .  $\kappa_{j,j}(\Delta l)$  is normalized to  $\kappa_{j,j}(0) = 1$ , and the spatial distance between the two modes (j, l) and (j, l') is  $D = L\Delta l$ , where L is the length of the sample. The results are obtained from 100 realizations of simulated Ly $\alpha$  transmitted flux. The central line is the mean and the upper and lower lines show the 95% confidence level. The result for QSO HS 1700+64 is displayed as the solid squares.

Fig. 5.— The  $\Delta l$ -dependence of correlation  $\kappa_{j,j+1}(\Delta l)$ . where  $\kappa_{j,j+1}(\Delta l)$  is normalized to  $\kappa_{j,j}(0) = 1$ , and the spatial distance between the two modes (j, l) and (j + 1, l') is  $D = L\Delta l$ , where L is the length of the sample. The results are obtained from 100 realizations of simulated Ly $\alpha$  transmitted flux. The central line is the mean and the upper and lower lines show the 95% confidence level. The result for QSO HS1700+64 is displayed as the solid squares.

Fig. 6.—  $\kappa_{j;j}(\Delta l)$  for the moderate resolution data of the Ly $\alpha$  forest lines LWT/JB. The case of l = l', or  $\Delta l = 0$ , is the localized case, and l' + l + 1 and l' = l + 2 show the non-local correlations.  $\kappa_{j;j}(\Delta l)$  is calculated for each QSO absorption line system and the 1- $\sigma$  bars are determined from the variance of the data consisting of all the systems.

Fig. 7.— Same as figure 4, but for the HU/KT high resolution absorption samples of  $Ly\alpha$  forest lines.

Fig. 8.— The correlation  $\kappa_{j,j+1}(\Delta l)$  vs.  $\Delta l = l' - l$  for the moderate resolution data of Ly $\alpha$  forest lines LWT/JB. As expected, there is no power in this second order scale-scale correlation at any scale.  $\kappa_{j;j+1}(\Delta l)$  is calculated for each QSO absorption line system and the 1- $\sigma$  bars determined from the variance of the data consisting of all the systems.

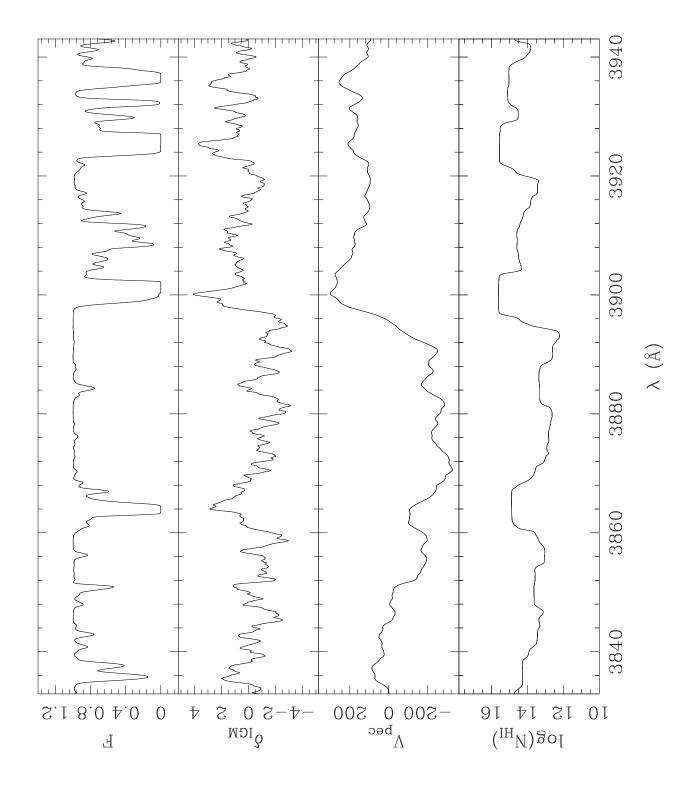
Fig. 9.— Same as figure 5 but now using the high resolution data HU/KT.

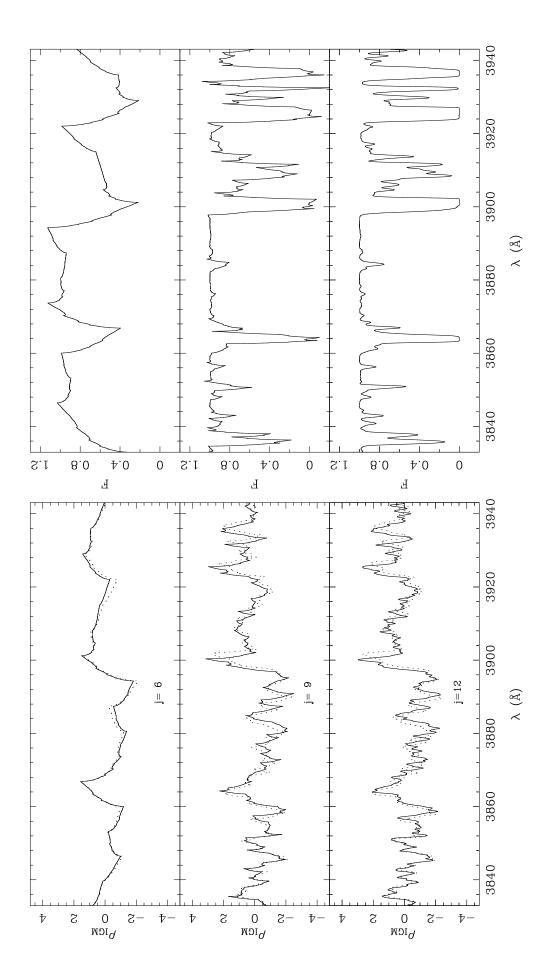
Fig. 10.— The 4th-order correlation  $Q_{j,j}^{2,2}(\Delta l)$  from 100 realizations of simulated Ly $\alpha$  transmitted flux and QSO HS1700+64. The spatial distance between the two modes (j, l) and (j, l') is  $D = L\Delta l$ , where L is the length of the sample. The central line is the mean and the upper and lower lines show 95% confidence level of the simulation samples. The result for the QSO HS1700+64 is displayed as the solid squares.

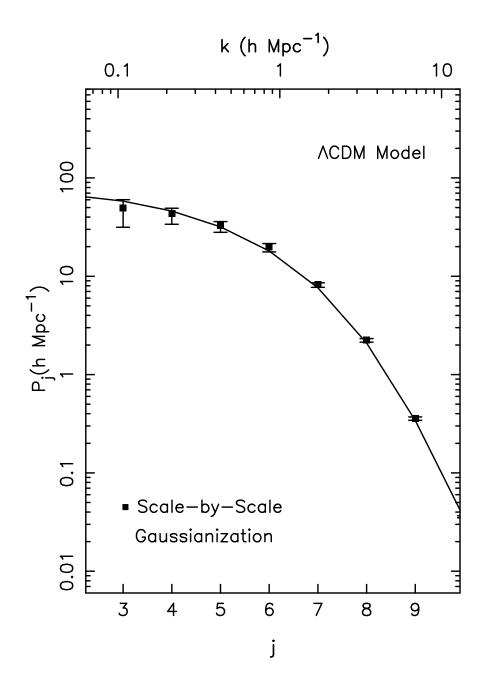
Fig. 11.— The 4th-order scale-scale correlation  $C_j^{2,2}(\Delta l)$  from 100 realizations of simulated Ly $\alpha$  transmitted flux and QSO HS1700+64. The spatial distance between the two modes (j, l) and (j + 1, l') is  $D = L\Delta l$ , where L is the length of the sample. The central line is the mean and the upper and lower lines show the 95% confidence level of the simulation samples. The result for the QSO HS1700+64 is displayed as the solid squares.

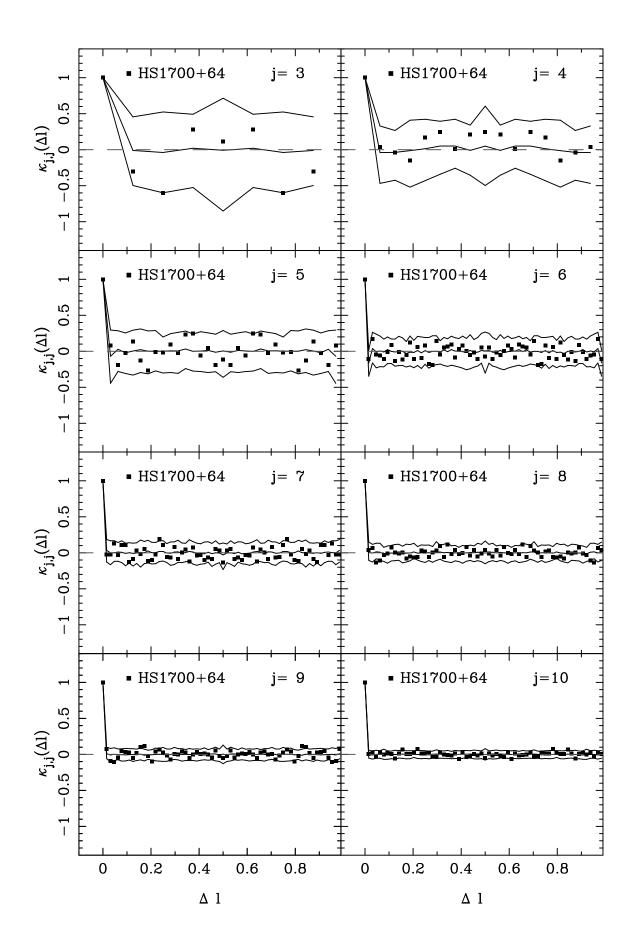
Fig. 12.— The 4th-order scale-scale correlations,  $C_j^{2,2}(\Delta l)$ , for the LWT/JB data.  $C_j^{2,2}(\Delta l)$  is calculated for each QSO absorption line system and the 2- $\sigma$  bars determined from the variance of the data consisting of all the systems.

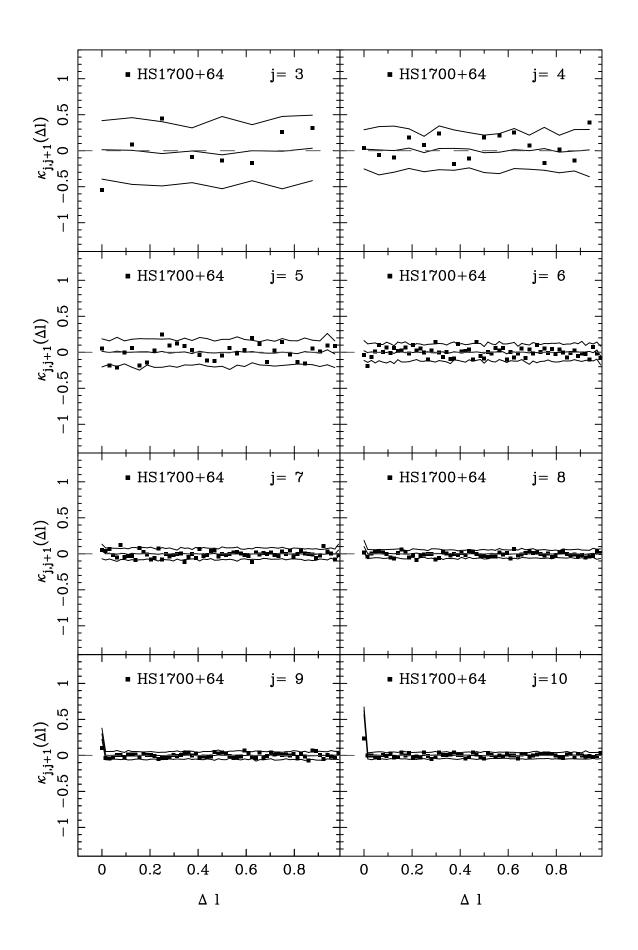
Fig. 13.— The 4th-order scale-scale correlations,  $C_j^{2,2}(\Delta l)$  for the HU/KT data.  $C_j^{2,2}(\Delta l)$  is calculated for each QSO absorption line system and the 2- $\sigma$  bars determined from the variance of the data consisting of all the systems.

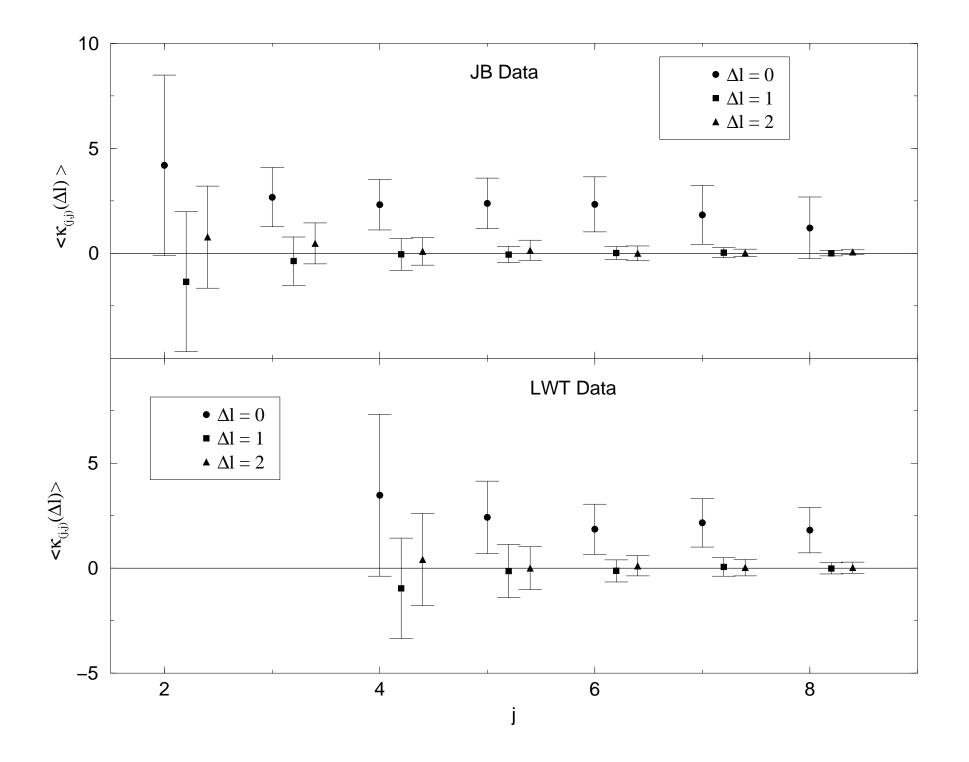


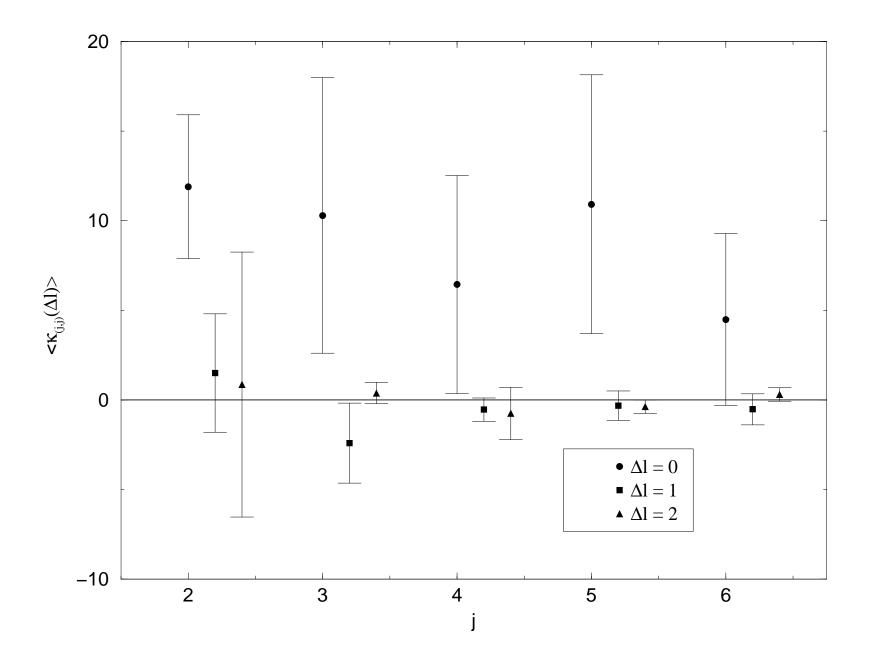


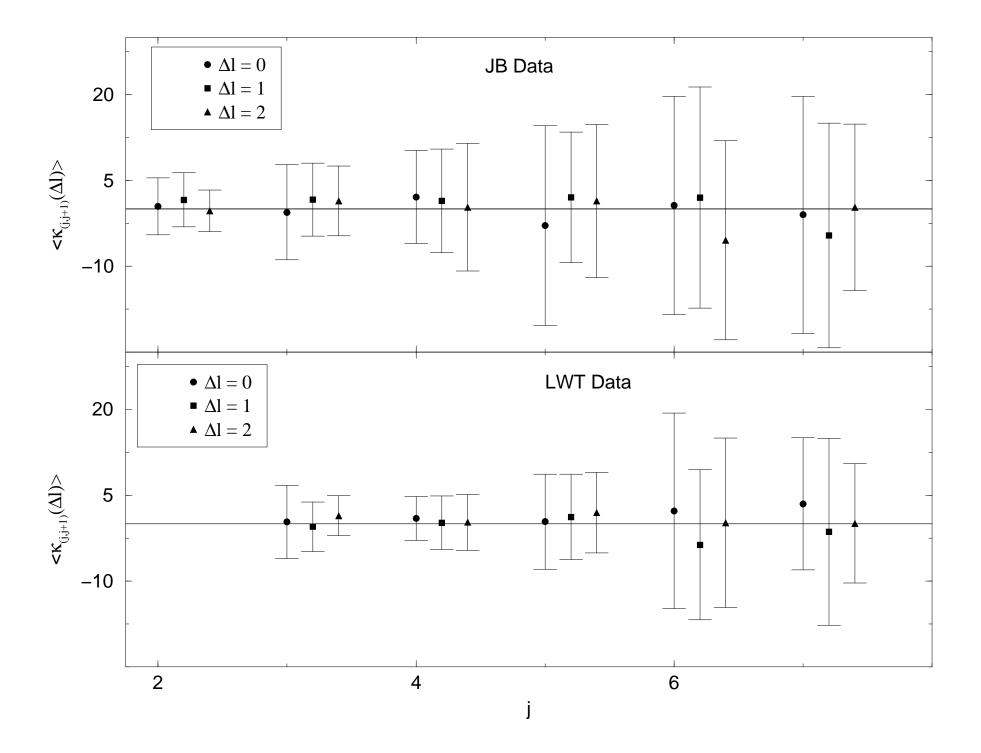


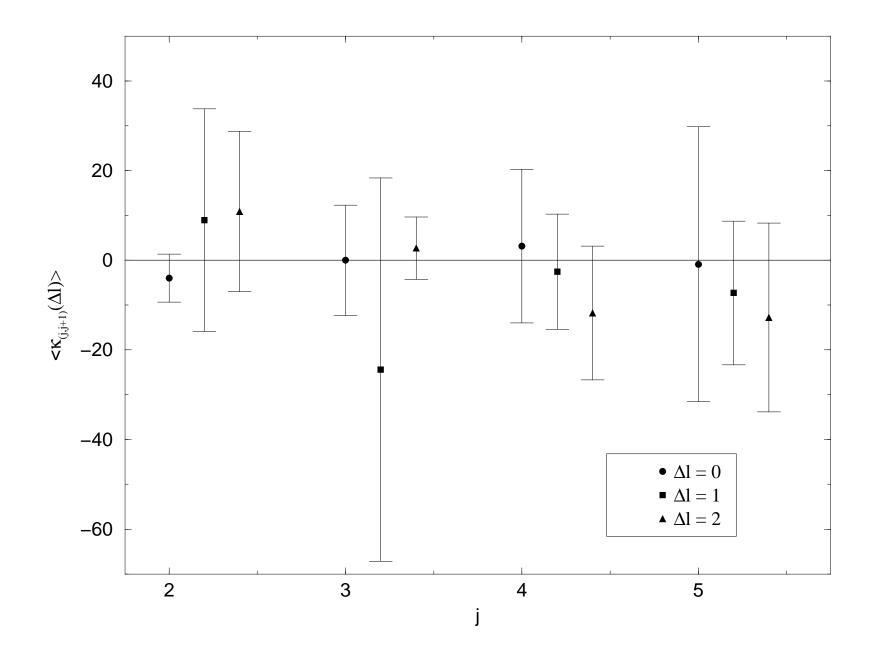


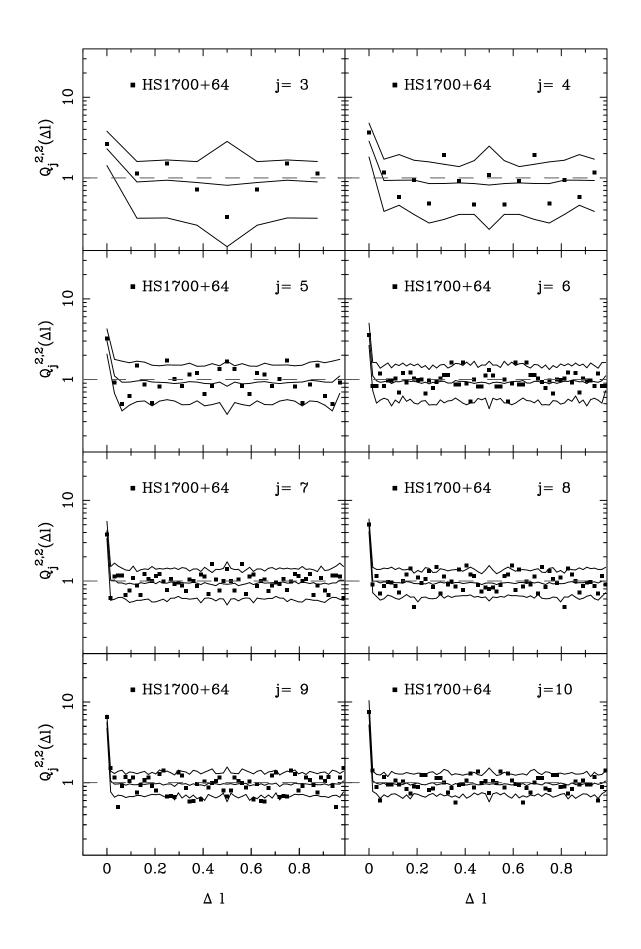


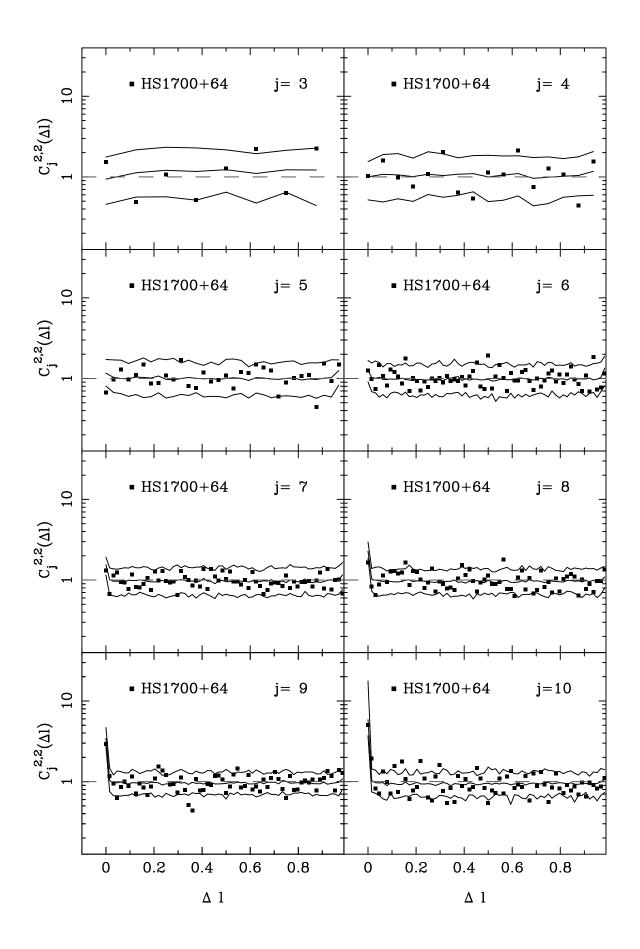


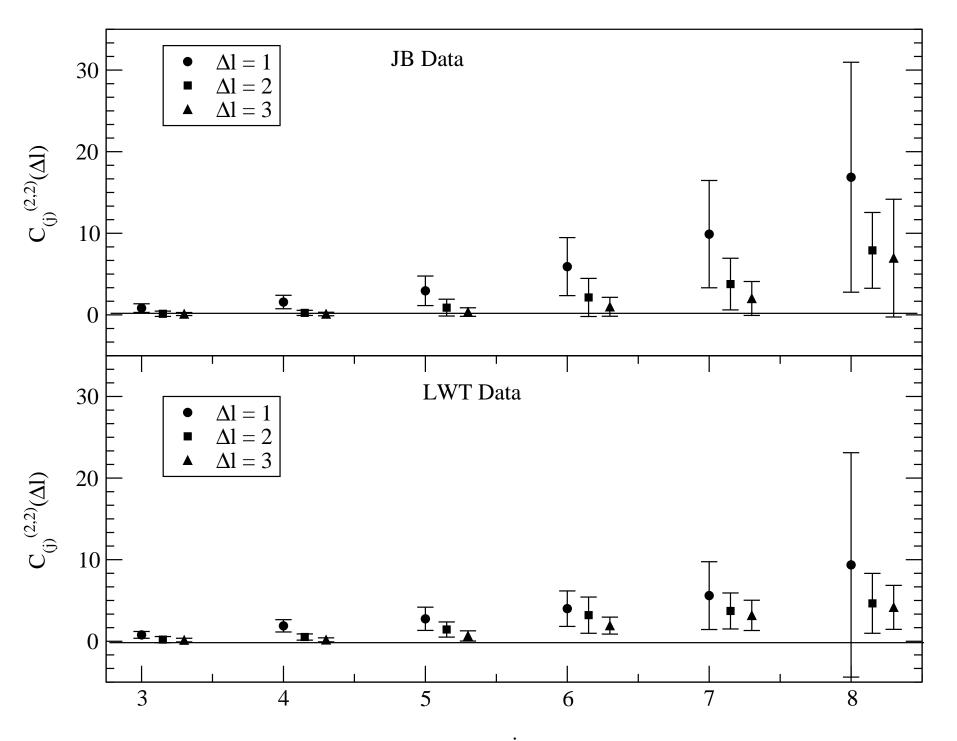




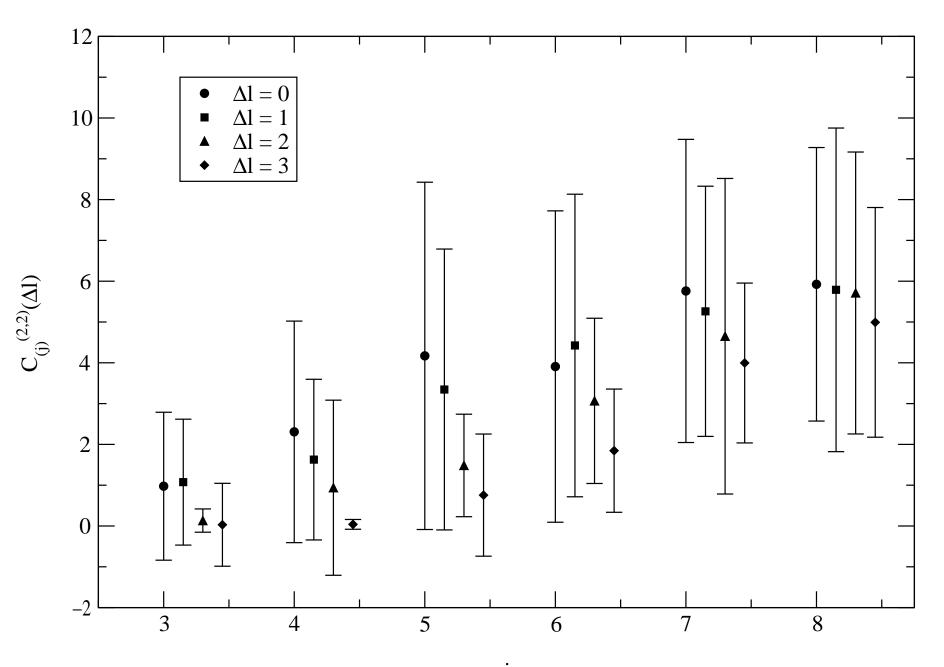








j



j